Wavelength Routers for Optical Networks-on-Chip Using Optimized Photonic Crystal Ring Resonators

Giovanna Calò
Vincenzo Petruzzelli

Wavelength Routers for Optical Networks-on-Chip Using Optimized Photonic Crystal Ring Resonators

Giovanna Calò and **Vincenzo Petruzzelli**

Dipartimento di Ingegneria Elettrica e dell'Informazione - Politecnico di Bari, Bari 70125, Italy

Abstract: In this paper, we propose an optical 1×2 passive wavelength router (λ-router), based on photonic crystal ring resonators. The router, as basic building block to be assembled into higher order routing matrices, exploits a broadband crossing between two photonic crystal waveguides and a photonic crystal ring resonator. Moreover, we analyze the behavior of a 4×4 λ-router configuration obtained by assembling eight 1×2 routers. The design criteria are pointed out, and the numerical results, obtained by the finite-difference time-domain and the plane-wave expansion methods, are reported. The 4×4 λ-router has a footprint of $30 \ \mu$m $\times 30 \ \mu$m, and it is capable of connecting four transmitters with four receivers with a maximum crosstalk between the ports equal to -13.9 dB.

Index Terms: Photonic Crystals, optical switches, photonic integrated circuits, optical interconnections.

1. Introduction

In an on-chip photonic communication network, different switching devices are assembled on the same chip to achieve the signal routing among N transmitters and N receivers. One of the most interesting applications of such integrated photonic networks is the communication among the different cores in chip multiprocessors (CMPs). A CMP consists of several smaller processing cores designed and replicated several times, which achieve performance gain through parallel code execution using multiple threads across the cores. The exchange of data among the different cores is indeed a critical issue, which can limit the performances of the overall system.

Nanotechnology has enabled the integration of a photonic layer into CMPs allowing the exploitation of the advantages of optical data transmission, such as high transmission bandwidth, low latency, low power consumption, etc. [1]. Different components must be integrated into the network to allow on-chip photonic communication, such as multiplexers/demultiplexers [2], filters [3]–[5], modulators [6]–[9], and switches [10]–[15]. Among all these components, the switch plays a fundamental role since it is the basic building block to be assembled into higher order matrices within the networks [16], [17]. The switch is capable of routing the signals along the network thus connecting the different processors.

The design of a photonic network can rely on two different approaches exploiting either active or passive switches. In the case of active switches, the switching mechanism is achieved by the

variation of the refractive index induced by an applied voltage, such as by thermo-optic or plasma-optic effects in silicon-based switches [18]–[20]. Networks exploiting active switches are reconfigurable, i.e., the signal path can be varied by varying the state of the switches, but the switching mechanism itself increases the total required power. Moreover, the path setup latency can be longer than the propagation time [21]. In fact, the time required for the path setup, i.e., the configuration of the states of the active switches along the path, is linked to the switching speed of the active device, which can be in the order of nanoseconds, whereas the light propagation time is about equal to 15 ps/mm in a silicon waveguide [21].

The second approach to design photonic NoCs relies on passive components in which the routing of the signal is promoted by the wavelength resonance mechanism [22]. The signal path depends on the wavelength of the input optical signal, and the routing is obliged by the resonant wavelengths of the routing devices encountered along the path. Therefore, the reconfigurability is achieved only by changing the wavelength of the input signal. Although passive components give less freedom in the reconfiguration of the network, the routing mechanism does not require additional power consumption, and the delay of the signal is only due to the propagation time.

In this paper, we propose a passive photonic crystal (PhC) router configuration exploiting a PhC ring resonator (PCRR). Thanks to the periodic modulation of the refractive index, PhC structures are able to inhibit the propagation of the light at given wavelengths, i.e., the photonic band gap (PBG). The appropriate perturbation of the index periodicity allows the localization of modes in the PBG and the realization of optical devices such as waveguides, cavities, and filters [23], [24]. Exploiting the different material properties, the PBG structures can lead to interesting devices such as efficient tunable filters and frequency converters, e.g., in the case of liquid crystal infiltration or nonlinear materials [25], [26]. Thanks to their capability of reducing the group velocity at certain wavelengths, PBGs also exhibit a more efficient interaction between the light and the active material [27], [28].

The light confinement in PhC devices is based on the PBG, which is more efficient in optical confinement with respect to the total internal reflection mechanism in conventional waveguides. Moreover, in conventional waveguides, the radiation loss increases exponentially with the reduction of the bending radius [29]. Therefore, PhCs allow to realize ultracompact devices such as cavities and bends and can be a valid alternative solution to waveguide-based components.

An interesting component, which conjugates the compactness of PhC devices with the versatility of waveguide ring resonators, is the PCRR made of a ring-shaped linear defect in a PhC lattice based on a square lattice of silicon rods in air. Different structures based of on rod lattices have been fabricated to implement different devices such as waveguides, directional couplers, and lasers [30]–[33]. Moreover, PCRRs have been successfully designed and fabricated to be used as ultracompact add–drop filters and modulators [29], [34], [35]. Here, we report the design of a PCRR 1×2 router, which behaves as a passive wavelength router (λ-router), to be assembled into higher order matrices as basic building block. The router is made of a broadband crossing between two PhC waveguides and of a PCRR.

We first report the results of the design and the analysis of this basic building block and of its constituent parts, i.e., the PCRR and the crossing. Moreover, we analyze the behavior of a 4×4 λ-router configuration obtained by assembling eight 1×2 routers. The design criteria are pointed out, and the numerical results, obtained by the finite-difference time-domain (FDTD) and plane-wave expansion (PWE) methods, are reported [36].

2. PCRR 1×2 Router

The basic routing element to be assembled into higher dimension matrices is the 1×2 router. The PhC 1×2 router, proposed in this paper, is shown in Fig. 1(a), and it is made of a broadband PhC waveguide crossing [see Fig. 1(b)] and a PCRR [see Fig. 1(c)], both suitable for the integration into the 4×4 λ-router, which will be described in the following.

The design is based on a 2-D PhC square lattice made of silicon rods in air. The refractive index of the rods is n = 3.47, whereas the lattice constant a = 0.540 μm and the rod radius r = 0.175 · a have
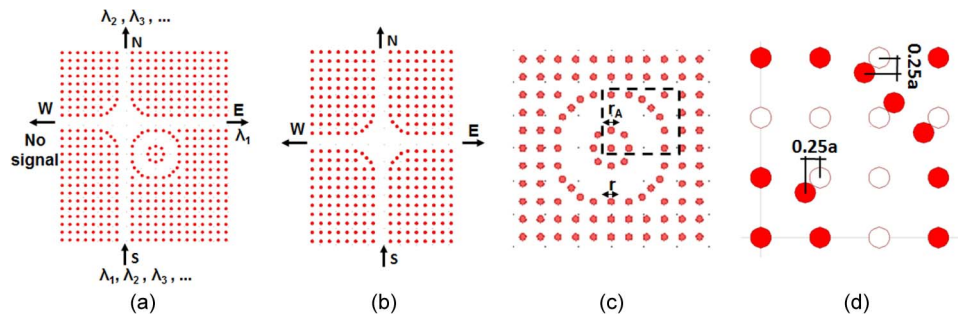
Fig. 1. (a) Scheme of the 1 × 2 PCRR router and of its constituent parts: (b) broadband PhC waveguide crossing, (c) PCRR, and (d) enlarged view of a portion of the PCCR with the original rod position, marked by the white circles, in the square lattice.

been chosen to achieve a PBG around the operation wavelength $\lambda = 1.55$ μm, extending from $\lambda = 1.2162$ μm to $\lambda = 1.7940$ μm (i.e., the normalized frequency a/λ ranging from 0.301 to 0.444). The PCRR is obtained by removing a series of rods to create a PhC waveguide ring. The rods along the ring perimeter are shifted of $0.25 \cdot a$ along the horizontal and vertical directions, with respect to the original lattice, to achieve a circular symmetry. Fig. 1(d) schematizes a portion of the PCRR evidencing, by white circles, the original position of the square lattice rods. The numerical results reported in the following sections are obtained by the PWE and by the bidimensional FDTD simulations. The structure is simulated by the FDTD method only in the horizontal plane, whereas it is considered as infinite in the vertical plane and possible radiation losses in the vertical direction are neglected. In actual fabricated devices, to achieve performances similar to the theoretical ones, the rod-type devices should require the realization of omnidirectional reflectors on and below the 2-D PhC structures to guarantee efficient light confinement in the vertical direction [31], [32], [37].

According to the scheme reported in Fig. 1(a), the optical signal launched at port S (South port) is transmitted at port E (East port) if its wavelength is coincident with one of the PCRR resonances (e.g., λ_1), whereas it is transmitted at port N (North port) for all the other wavelengths (e.g., $\lambda_2, \lambda_3, \ldots$) and no signal comes out at port W (West port). The 1 × 2 router behavior is reciprocal in the sense that the signal launched at port E comes out at port S at the PCRR resonant wavelength, whereas it is transmitted at port W otherwise.

The basic 1 × 2 routing element proposed in this paper is meant to be exploited to create 4 × 4 matrices or even in higher order matrices (N × N) capable of connecting N inputs with N outputs. In a wavelength router, the number of wavelengths necessary for the signal routing increases with the number of transmitters and receivers to be connected, e.g., the number of processors exchanging data over a photonic NoC. Therefore, the PCRRs in the matrix must be suitably designed to resonate at different wavelengths. Moreover, the crossing must be broadband to allow the transmission to port N of all the nonresonant wavelengths.

In the following, we will first analyze the behavior of the broadband crossing, and then, we will report the study of the PCRR behavior as a function of the geometrical parameters.

2.1. Broadband PhC Waveguide Crossing

The ability to intersect waveguides with low crosstalk is crucial in constructing optical circuits. Different configurations have been proposed in the literature to achieve such a goal. In particular, crossings between PhC waveguides exploiting either resonant cavities or multimode interference (MMI) have been proposed in [38]–[40] exhibiting low values of crosstalk.

The crossing configuration proposed in this paper, shown in Fig. 1(b), was achieved by optimizing the position of the dielectric rods near the crossing. In particular, the rods were shifted of $0.25 \cdot a$ along the horizontal and vertical directions accordingly to the scheme shown in Fig. 1(d), which is also valid for the crossing. This configuration is not only suitable for the integration with the PCRR geometry but also permits a broadband operation.
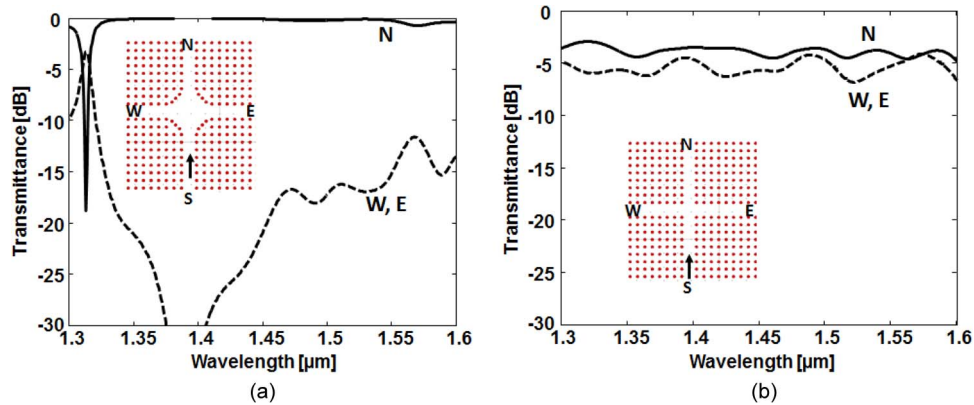
Fig. 2. Transmittance spectra at the different ports (E, W, N) when the signal is launched at the S input port (a) for the proposed crossing configuration and (b) for a simple PhC waveguide crossing. The device geometries are as in the insets.

The behavior of the crossing was analyzed by 2-D FDTD simulations considering a Gaussian pulse launched as input signal. Fig. 2(a) shows the transmittance at the different ports (E, W, and N) when the signal is launched at the S input port for the proposed crossing configuration. The transmittance spectra were calculated normalizing the transmitted power at the output ports (i.e., E, W, and N) to the input power at port S. For the sake of comparison, Fig. 2(b) shows the transmittances for the simple crossing between two PhC waveguides, shown in the inset of Fig. 2(b).

The simple waveguide crossing [see Fig. 2(b)] exhibits a noticeable crosstalk among the output ports, which makes this simple geometry unsuitable for any practical use in photonic networks. Conversely, Fig. 2(a) shows that, for the proposed configuration, the signals at the isolated ports (E and W) are well below the transmitted signal at the through port (N) almost in all the considered wavelength range. The results shown in Fig. 2 were obtained considering the input signal launched at port S. However, the behavior is similar if the other ports are considered as inputs.

The crosstalk between the different ports can be calculated in decibels as $CT_{i,j} = T_j - T_i$ where i and j corresponds to W, N, E, and S, whereas T_i and T_j denote the transmittances at the through and isolated ports, respectively, expressed in decibels. Accordingly, we can define the operation bandwidth of the crossing as the wavelength range in which the crosstalk is below a given reference value. For example, if the reference value is chosen to be equal to $CT = CT_{NE} = CT_{NW} = -10$ dB, according to Fig. 2(a), the bandwidth is equal to $\Delta\lambda = 280$ nm (i.e., from $\lambda = 1.32$ μm to $\lambda = 1.60$ μm). If more stringent crosstalk constraints are required, a narrower bandwidth must be considered. The minimum crosstalk value $CT < -30$ dB is achieved in a 32-nm bandwidth around the wavelength $\lambda = 1.39$ μm. These performances are comparable with those ($CT < -30$ dB in a 60-nm bandwidth) reported for wire waveguide elliptical crossings [42]. In the following, we will report the results of the λ-router configuration operating between $\lambda = 1.48$ μm and $\lambda = 1.55$ μm, where the crossing exhibits a crosstalk below -16 dB.

2.2. PCRR Resonant Modes

The PCRR 1 × 2 router proposed in this paper exploits a PCRR, shown in Fig. 1(c), which is obtained by removing a series of rods to create a PhC waveguide ring. The rods along the ring perimeter are shifted to achieve a circular symmetry, which is better suited for the integration with the broadband crossing. The radius of the central rods r_A can be varied to tune the wavelength of the resonant modes, whereas all the other rods have a fixed radius $r = 0.175 \cdot a$.

The resonant modes supported by the PCRR were first analyzed by the PWE technique [36]. Fig. 3 shows the patterns of the electric-field intensity of the resonant modes calculated for the PCRR having radius of the central rods equal to $r_A = r = 0.175 \cdot a$. The different modes are
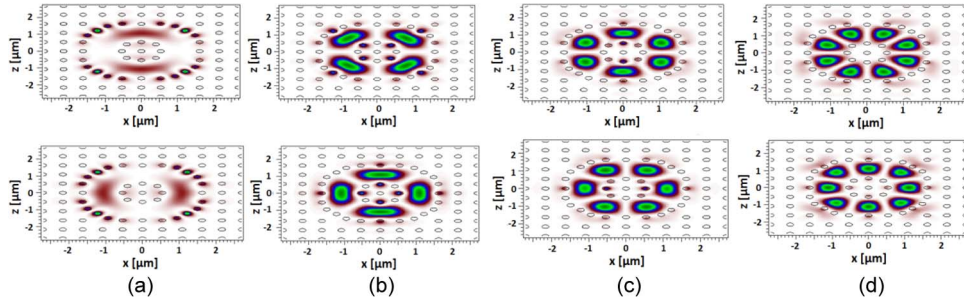
Fig. 3. Pattern of the electric-field intensity of the PCRR resonant modes: (a) dipole, (b) quadrupole, (c) hexapole, and (d) octupole. Each mode shows a double degeneracy.

TABLE 1

Normalized frequencies of the PCRR resonant modes for central rod radius $r_A = r$

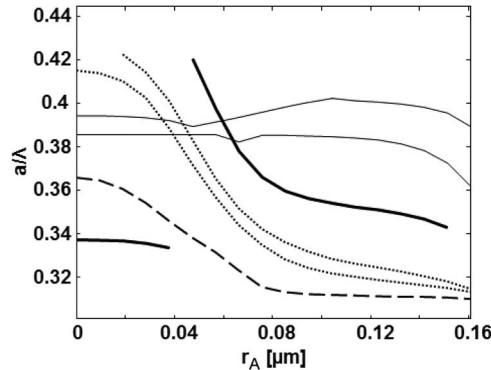| Type of mode	Resonant frequency a/λ_1	Resonant frequency a/λ_2
Dipole	0.312307	0.313475
Quadrupole	0.324407	0.331765
Hexapole	0.356324	0.356419
Octupole	0.384396	0.401818

Fig. 4. Normalized frequency a/λ of the different resonant modes as a function of the central rod radius r_A for the dipole (dashed curves), the quadrupole (dotted curves), the hexapole (thick solid curves), and the octupole (thin solid curves).

characterized by the number of lobes in the field profile. In particular, Fig. 3 shows the (a) dipole, (b) quadrupole, (c) hexapole, and (d) octupole modes, each characterized by a double degeneracy. The normalized frequencies (a/λ_1 and a/λ_2) of the two degenerate resonant modes shown in Fig. 3 are reported in Table 1.

By varying the radius r_A of the central rods, a shift in the frequency of the PCRR resonances can be achieved. Fig. 4 shows the normalized frequency a/λ of the different resonant modes as a function of the central rod radius r_A for the dipole (dashed curves), the quadrupole (dotted curves), the hexapole (thick solid curves), and the octupole (thin solid curves). From Fig. 4, we can observe that the curves pertaining to the two degenerate modes for the dipole (dashed curve) and hexapole (thick solid curve) patterns are completely coincident, whereas the two degenerate modes in the case of the quadrupole (dotted curves) and of the octupole (thin solid curves) have slightly different resonant wavelength values.
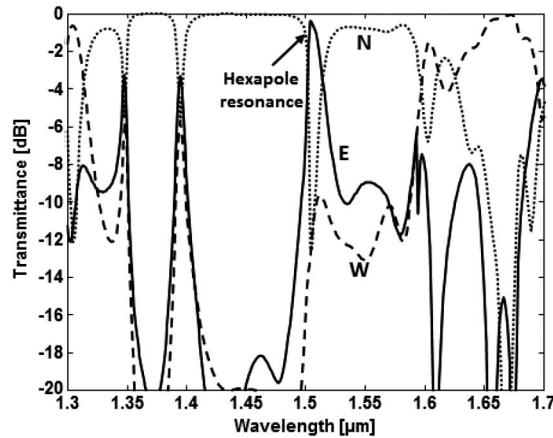
Fig. 5. Transmittance in dB for the PCRR 1 × 2 router at the East E (solid curve), West W (dashed curve), North N (dotted curve) ports, when the input signal is launched at the South S port. The radius of the PCRR central rods is equal to $r_A = 0.175 \cdot a$. The resonance of the hexapole mode occurs at $\lambda = 1.5060 \ \mu$m.

According to Fig. 4, the resonant wavelength of the different modes can be tailored by properly choosing the central rod radius.

2.3. PCRR 1 × 2 Router: Numerical Results

The PCRR 1 × 2 router, shown in Fig. 1(a), was analyzed by the FDTD simulations considering a Gaussian pulse launched as input signal at the south (S) port. Fig. 5 shows the transmittance spectra calculated at the East E (solid curve), West W (dashed curve), and North N (dotted curve) output ports. In this case, the radius of the central rods is equal to $r_A = r = 0.175 \cdot a = 0.094 \ \mu$m. The transmittance spectra are calculated normalizing the transmitted power at the output ports, i.e., E, W, and N, to the input power at port S.

From Fig. 5, we can observe that, at the wavelength $\lambda = 1.5060 \ \mu$m, the signal is almost completely transferred to port E (transmittance $T \cong -0.5$ dB), whereas the signals transmitted at ports W and N are about equal to $T \cong -12.0$ dB. This condition occurs at the resonance wavelength of the hexapole modes which give the maximum value of transmittance at port E. Two other maxima of the transmittance spectrum at port E (solid curve) occur in correspondence of the two octupole resonant modes, i.e., at $\lambda = 1.3548 \ \mu$m and $\lambda = 1.3950 \ \mu$m, with transmittance equal to $T = -3.3$ dB. At the same wavelengths, the transmittances at ports W and N are about equal to $T \cong -6.0$ dB thus giving a much higher crosstalk between the router ports with respect to the case of the hexapole resonant modes. The other resonant modes, i.e., dipole and quadrupole, are not capable of routing the signal coming from the south port to the east one.

On the basis of the aforesaid considerations, for the design of the 1 × 2 router and of the overall λ-router, we will refer to the hexapole resonant modes, which are the dominant ones in the sense that they give the maximum transmittance at port E.

As mentioned before, the resonance wavelength of the resonant mode can be varied by changing the radius r_A of the PCRR central rods. Fig. 6 shows the resonance wavelength of the hexapole resonant mode as a function of the central rod radius r_A calculated by the PWE technique applied to the only PCRR (solid curve) and evaluated from the transmittance spectra of the PCRR 1 × 2 router by the FDTD simulations (dots). A good agreement is apparent.

As mentioned before, the crosstalk between the different ports can be calculated in dB as $CT_{i,j} = T_j - T_i$ where i and j corresponds to W, N, E, and S, whereas T_i and T_j denote the transmittances at the through and at the isolated ports, respectively, expressed in decibels. Similarly, the insertion loss can be calculated as $IL = -T_i$ where T_i is the through port transmittance expressed in decibels. The insertion loss IL and the worst-case crosstalk CT, calculated at the
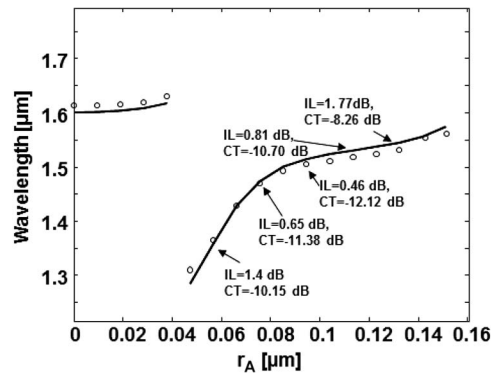
Fig. 6. Resonance wavelength of the hexapole resonant mode as a function of the central rod radius r_A calculated by the PWE technique applied to the only PCRR (solid curve) and evaluated from the transmittance spectra of the PCRR 1 × 2 router by the FDTD (dots). The Insertion loss IL and the worst-case crosstalk CT, calculated at the hexapole resonance peak by the FDTD are also shown.
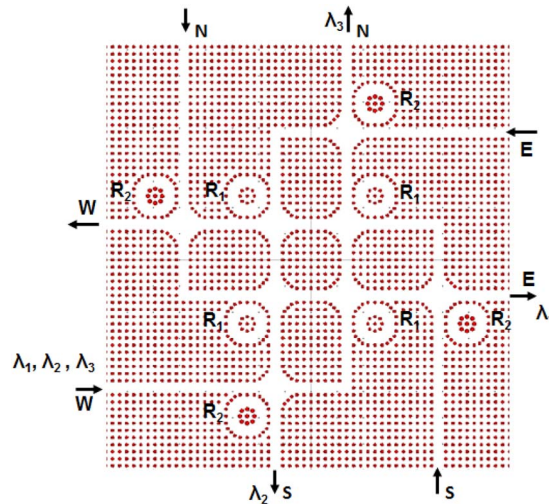

Fig. 7. Scheme of the 4 × 4 PCRR λ-router. The input and output ports are denoted by the arrow directions. According to its wavelength the input signal is routed to the different output ports.

hexapole resonance peak by the FDTD, are also shown in Fig. 6. At the hexapole resonance wavelength, which varies with the central rod radius r_A as shown in Fig. 6, the through port is E, whereas N and W are the isolated ones.

From Fig. 6, we can infer that the rod radius values ranging from $r_A \cong 0.05$ μm to $r_A \cong 0.14$ μm are more suitable for the 1 × 2 router design, since they correspond to a wider variation of the resonance wavelength that allows better tailoring the routing behavior. In fact, as shown in Fig. 6, for radius values $r_A < 0.04$ μm, the resonance wavelength is always around $\lambda = 1.6$ μm, whereas it varies from $\lambda = 1.3$ μm to $\lambda = 1.55$ μm otherwise. Aiming at considering wider matrices, in which the routing mechanism is promoted by the wavelength diversity, in the following, we will restrict the choice of the rod radius values in the range between $r_A \cong 0.05$ μm and $r_A \cong 0.14$ μm.

3. PCRR 4 × 4 λ-Router

Fig. 7 shows a scheme of the proposed PCRR λ-router which behaves as a 4 × 4 router matrix. The chosen router matrix topology is a PhC version of the configuration reported in [41], where conventional waveguide components were used, i.e., crossings, bends, and ring resonators. As

TABLE 2

Links between the input and output ports according to the wavelength of the input signal

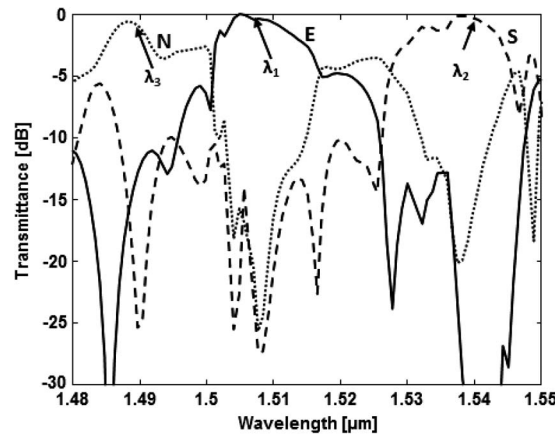| Input	Output			
	W	N	E	S
W	-	λ_3	λ_1	λ_2
N	λ_2	-	λ_3	λ_1
E	λ_1	λ_2	-	λ_3
S	λ_3	λ_1	λ_2	-

Fig. 8. Transmittance spectra calculated at the East E (solid curve), South S (dashed curve), North N (dotted curve) output ports considering a Gaussian pulse launched as input signal at the West (W) input port.

schematized in Fig. 7, the overall structure is made by the repetition of the basic building block, made by a PCRR and a crossing which build up the 1×2 routing structure analyzed in the previous sections. The different building blocks are interconnected by simple PhC waveguides and bends. Indeed, other matrix topologies based on the connection of multiple basic building blocks (i.e., the 1×2 router) are also possible. Moreover, by adding a second PCRR disposed near the crossing, according to radial symmetry with respect to the first one, a 2×2 router can be obtained, thus opening up new possibilities for higher order matrix configurations.

The matrix has four input and four output ports denoted as North (N), South (S), East (E), and West (W). Each input port can be connected to each output one according to the wavelength of the input signal.

This behavior can be achieved since different PCRRs are used, which resonate at different wavelengths. In particular, the PCRRs having central rod radius $r_A = R_1$ resonate at λ_1, whereas those with radius $r_A = R_2$ resonate at a different wavelength λ_2. As an example, if a signal at wavelength λ_1 is launched at the input port West it comes out at the output port East, it being deviated by the resonant PCRR with rod radius R_1. Similarly, if a signal λ_2 is launched at the West input port, it is routed to the South output port by the resonant PCRR with rod radius R_2. Finally, if a third wavelength value λ_3 is used, for which none of the PCRRs is in the resonant condition, the signal is transmitted at the output port North.

Table 2 reports the possible links between the input and output ports according to the wavelength of the launched signal. In the λ-router operation, those links corresponding to coincident input and outputs are neglected.

On the basis of the analysis of the PCRR 1×2 router, two values of the central rod radius r_A were chosen to build up a λ-router working around the wavelength $\lambda_2 = 1.5$ μm: $r_A = R_1 = 0.175 \cdot a = 0.094$ μm and $r_A = R_2 = 0.250 \cdot a = 0.135$ μm, which give two different resonance wavelengths $\lambda_1 = 1.5060$ μm and $\lambda_2 = 1.5400$ μm, respectively.

Fig. 8 shows the transmittance spectra calculated at the East E (solid curve), South S (dashed curve), and North N (dotted curve) output ports considering a Gaussian pulse launched as input signal at the West (W) input port. For the sake of clarity, the spectra are shown in a restricted wavelength range (i.e., $\lambda = 1.48$ μm and $\lambda = 1.55$ μm) around the routing operation wavelengths. At $\lambda_1 = 1.5060$ μm, the PCRR with central rod radius equal to $R_1 = 0.094$ μm resonates, and the signal is almost completely transferred to port E (transmittance $T = -0.1$ dB), whereas the signals transmitted at ports S and N are about equal to $T \cong -14.0$ dB and $T \cong -17.0$ dB, respectively. Moreover, at $\lambda_2 = 1.5400$ μm, the PCRR with central rod radius equal to $R_2 = 0.135$ μm resonates and the signal is almost completely transferred to port S (transmittance $T \cong -0.3$ dB), whereas the signals transmitted at ports E and N are about equal to $T \cong -16.0$ dB and $T \cong -45.0$ dB, respectively. Finally, the maximum transmittance at port N occurs at the wavelength $\lambda_3 = 1.4880$ μm with $T = -0.6$ dB. At the same wavelength $\lambda_3 = 1.4880$ μm, the signals transmitted at ports S and E are about equal to $T \cong -16.0$ dB.

Considering the results reported in Fig. 8, at $\lambda_1 = 1.5060$ μm, the through port is E, whereas the isolated ones are S and N. Therefore, the crosstalk values between the different ports are equal to $CT_{S,E} = -13.9$ dB and $CT_{N,E} = -16.9$ dB. Similarly, at $\lambda_2 = 1.5400$ μm, the through port is S, whereas the isolated ones are E and N. Therefore, the crosstalk values between the different ports are equal to $CT_{E,S} = -15.7$ dB and $CT_{N,S} = -44.7$ dB. Finally, at $\lambda_3 = 1.4880$ μm, the through port is N, whereas the isolated ones are S and E, giving crosstalk values equal to $CT_{S,N} = CT_{E,N} = -15.4$ dB. Owing to the λ-router symmetry, similar spectra are obtained when the other ports are considered as inputs. The crosstalk performances are comparable with the ones achieved by optical routers based on conventional ring resonators [22], [43]. Moreover, the full-width half-maximum (FWHM) bandwidth of the transmission peaks is about equal to $\Delta\lambda = 16$ nm. Considering Fig. 6, by varying the central rod radius from $r_A \cong 0.05$ μm to $r_A \cong 0.14$ μm, the resonance wavelength can be varied in a 250-nm wavelength range (i.e., $\lambda = 1.3$ μm to $\lambda = 1.55$ μm), and therefore, virtually, 15 resonances with $\Delta\lambda = 16$ nm could be considered. This would allow building larger matrixes provided the suitable choice of the resonance wavelengths according to the minimization of both the CT and the IL. For example, following a composition approach similar to the one reported in [44] and [45], the 8 $\times$ 8 configuration would require the allocation of seven wavelengths suitably chosen among the possible ones.

From the system level point of view, the 4 $\times$ 4 matrix could be regarded as a black box capable of passively routing a signal in the four directions (i.e., N, S, E, and W) but not allowing self-communications. Building blocks with similar characteristics, based on conventional ring resonators, have been assembled in different passive network topologies. As an example, in [44] and [45], a building block with similar routing capabilities, namely, the 4 $\times$ 4 Generic Wavelength-routed Optical Router (GWOR), was replicated several times to build up a N $\times$ N GWOR network in which the routing patterns are statically set at the design time by properly choosing multiple (i.e., $N - 1$) resonant wavelengths. Other possible configurations for passive wavelength routed networks are the folded crossbar and the snake topologies, based on the replication of 1 $\times$ 2 and 2 $\times$ 2 basic building blocks [45], [46]. All-optical wavelength-routed on-chip interconnects have been demonstrated to be, when optimally designed, power efficient and performance competitive with respect to actively routed networks [44]–[47].

Nonetheless, in the proposed routing configuration, the active routing could also be achieved, as proposed in [29] and [34], by perturbing the refractive index of the semiconductor (e.g., by plasma dispersion effect or by infiltration of electro-optic polymers) in the air-hole lattice structures. Although these active configurations can be technologically challenging, they could open up new possibilities for the investigation of network topology based on PCRRs.

The propagation delays values $\Delta t_1 \cong 0.2$ ps, $\Delta t_2 \cong 0.1$ ps, and $\Delta t_3 = 0.2$ ps were evaluated for the signal paths from port W to ports E, S, and N, respectively. These delay values were calculated from the FDTD simulations, considering the time necessary for a continuous-wave input signal at port W to reach the different output ports (i.e., ports E, S, and N at λ_1, λ_2, and λ_3, respectively).

4. Conclusion

A 1×2 PCRR router configuration has been proposed and analyzed through numerical simulations based on the PWE and FDTD models. The designed router behaves as a passive wavelength router, and it is a basic building block to be assembled into higher order matrices. The design curves necessary to correctly tune the PCRR resonances are obtained by varying the radius r_A of the PCRR central rods. Moreover, the results of the FDTD simulations of a 4×4 matrix made of eight 1×2 routers are reported.

The device is capable of connecting 4 transmitters and 4 receivers, e.g., the processors in a CMP, with a maximum crosstalk between ports equal to -13.9 dB. Thanks to the PhC capability of confining light, the proposed devices are very compact. In fact, the PCRR has a diameter equal to 4 μm, whereas the overall size of the 4×4 λ-router is about 30 μm $\times$ 30 μm and it exhibits subpicosecond propagation delays along the different signal routing paths.

Acknowledgment

References

[1] A. Biberman and K. Bergman, "Optical interconnection networks for high-performance computing systems," *Rep. Progr. Phys.*, vol. 75, no. 4, p. 046402, Apr. 2012.

[2] B. Kumar, V. Suthar, K. S. Kumar, and A. Singh, "Tunable wavelength demultiplexer for DWDM application using 1-D photonic crystal," *Progr. Electromagn. Res. Lett.*, vol. 33, pp. 27–35, 2012.

[3] C.-J. Wu, M.-H. Lee, W.-H. Chen, and T.-J. Yang, "A mid-infrared multichanneled filter in a photonic crystal heterostructure containing negative-permittivity materials," *J. Electromagn. Waves Appl.*, vol. 25, no. 10, pp. 1360–1371, Jan. 2011.

[4] G. Calò, A. Farinola, and V. Petruzzelli, "Equalization in photonic bandgap multiwavelength filters by the Newton binomial distribution," *J. Opt. Soc. Amer. B*, vol. 28, no. 7, pp. 1668–1679, Jul. 2011.

[5] G. Calò, D. Alexandropoulos, and V. Petruzzelli, "Active WDM filter on dilute nitride quantum well photonic band gap waveguide," *Progr. Electromagn. Res. Lett.*, vol. 35, pp. 37–49, 2012.

[6] W. M. J. Green, M. J. Rooks, L. Sekaric, and Y. A. Vlasov, "Ultra-compact, low RF power, 10 Gb/s silicon Mach–Zehnder modulator," *Opt. Exp.*, vol. 15, no. 25, pp. 17 106–17 113, Dec. 2007.

[7] Q. Xu, S. Manipatruni, B. Schmidt, J. Shakya, and M. Lipson, "12.5 Gbit/s carrier-injection-based silicon microring silicon modulators," *Opt. Exp.*, vol. 15, no. 2, pp. 430–436, Jan. 2007.

[8] A. Liu, L. Liao, D. Rubin, H. Nguyen, B. Ciftcioglu, Y. Chetrit, N. Izhaky, and M. Paniccia, "High-speed optical modulation based on carrier depletion in a silicon waveguide," *Opt. Exp.*, vol. 15, no. 2, pp. 660–668, Jan. 2007.

[9] D. J. Thomson, F. Y. Gardes, Y. Hu, G. Mashanovich, M. Fournier, P. Grosse, J-M. Fedeli, and G. T. Reed, "High contrast 40 Gbit/s optical modulation in silicon," *Opt. Exp.*, vol. 19, no. 12, pp. 11 507–11 516, Jun. 2011.

[10] B. G. Lee, A. Biberman, P. Dong, M. Lipson, and K. Bergman, "All-optical comb switch for multiwavelength message routing in silicon photonic networks," *IEEE Photon. Technol. Lett.*, vol. 20, no. 10, pp. 767–769, May 2008.

[11] J. Van Campenhout, W. M. J. Green, S. Assefa, and Y. A. Vlasov, "Low-power, 2×2 silicon electro-optic switch with 110-nm bandwidth for broadband reconfigurable optical networks," *Opt. Exp.*, vol. 17, no. 26, pp. 24 020–24 029, Dec. 2009.

[12] J. Van Campenhout, W. M. J. Green, and Y. A. Vlasov, "Design of a digital, ultra-broadband electro-optic switch for reconfigurable networks-on-chip," *Opt. Exp.*, vol. 17, no. 26, pp. 23 793–23 808, Dec. 2009.

[13] G. Calò, D. Alexandropoulos, A. D'Orazio, and V. Petruzzelli, "Wavelength selective switching in dilute nitrides multi quantum well photonic band gap waveguides," *Phys. Stat. Sol. (B) Basic Res.*, vol. 248, no. 5, pp. 1212–1215, May 2011.

[14] G. Calò, D. Alexandropoulos, and V. Petruzzelli, "Active photonic band-gap switch based on GaInNAs multiquantum well," *IEEE Photon. J.*, vol. 4, no. 5, pp. 1936–1946, Oct. 2012.

[15] G. Calò, A. D'Orazio, and V. Petruzzelli, "Broadband Mach–Zehnder switch for photonic networks on chip," *J. Lightw. Technol.*, vol. 30, no. 7, pp. 944–952, Apr. 2012.

[16] M. Yang, W. M. J. Green, S. Assefa, J. Van Campenhout, B. G. Lee, C. V. Jahnes, F. E. Doany, C. L. Schow, J. A. Kash, and Y. A. Vlasov, "Non-blocking 4×4 electro-optic silicon switch for on-chip photonic networks," *Opt. Exp.*, vol. 19, no. 1, pp. 47–54, Jan. 2011.

[17] G. Calò and V. Petruzzelli, "WDM performances of two- and three-waveguide Mach–Zehnder switches assembled into 4×4 matrix router," *Progr. Electromagn. Res. Lett.*, vol. 38, pp. 1–16, 2013.

[18] A. V. Tsarev, F. De Leonardis, and V. M. N. Passaro, "Thin heterogeneous SOI waveguides for thermooptical tuning and filtering," *Opt. Exp.*, vol. 16, no. 5, pp. 3101–3113, Mar. 2008.

[19] V. M. N. Passaro and F. Dell'Olio, "Scaling and optimization of MOS optical modulators in nanometer SOI waveguides," *IEEE Trans. Nanotechnol.*, vol. 7, no. 4, pp. 401–408, Jul. 2008.

[20] G. Calò and V. Petruzzelli, "Photonic interconnects for chip multiprocessing architectures," presented at the Proc. 14th ICTON, Jul. 2–5, 2012.

[21] A. Shacham, K. Bergman, and L. P. Carloni, "On the design of a photonic network-on-chip," in *Proc. 1st Int. Symp. NOCS*, 2007, pp. 53–64.

[22] A. Kazmierczak, W. Bogaerts, E. Drouard, F. Dortu, P. Rojo-Romeo, F. Gaffiot, D. Van Thourhout, and D. Giannone, "Highly integrated optical 4 × 4 crossbar in silicon-on-insulator technology," *J. Lightw. Technol.*, vol. 27, no. 6, pp. 3317–3323, Aug. 2009.

[23] J. D. Joannopoulos, R. D. Meade, and J. N. Winn, *Photonic Crystals: Molding The Flow of Light,* 2nd ed. Princeton, NJ, USA: Princeton Univ. Press, 2008.

[24] G. Calò, M. Grande, D. Alexandropoulos, and V. Petruzzelli, "Photonic band gap active waveguide filters based on dilute nitrides," *Phys. Stat. Sol. (C)*, vol. 10, no. 4, pp. 567–572, Apr. 2013.

[25] G. Calò, A. D'Orazio, M. De Sario, L. Mescia, V. Petruzzelli, and F. Prudenzano, "Tunability of photonic band gap notch filters," *IEEE Trans. Nanotechnol.*, vol. 7, no. 3, pp. 273–284, May 2008.

[26] R. Cowan and J. F. Young, "Mode Matching for second-harmonic generation in photonic crystal waveguides," *Phys. Rev. B*, vol. 65, no. 8, p. 085106, Feb. 2002.

[27] J. M. Bendickson, J. P. Dowling, and M. Scalora, "Analytic expressions for the electromagnetic mode density in finite, one- dimensional, photonic band-gap structures," *Phys. Rev. E*, vol. 53, no. 4, pp. 4107–4121, Apr. 1996.

[28] G. Calò, V. Petruzzelli, L. Mescia, and F. Prudenzano, "Study of gain in photonic band gap active InP waveguides," *J. Opt. Soc. Amer. B*, vol. 26, no. 12, pp. 2414–2422, Dec. 2009.

[29] Z. Qiang, W. Zhou, and R. A. Soref, "Optical add–drop filters based on photonic crystal ring resonators," *Opt. Exp.*, vol. 15, no. 4, pp. 1823–1831, Feb. 2007.

[30] S. Assefa, P. T. Rakich, P. Bienstman, S. G. Johnson, G. S. Petrich, J. D. Joannopoulos, L. A. Kolodziejski, E. P. Ippen, and H. I. Smith, "Guiding 1.5 μm light in photonic crystals based on dielectric rods," *Appl. Phys. Lett.*, vol. 85, no. 25, pp. 6110–6112, Dec. 2004.

[31] W. Y. Chiu, T. W. Huang, Y. H. Wu, F. H. Huang, Y. J. Chan, C. H. Hou, H. T. Chien, C. C. Chen, S. H. Chen, and J. I. Chyi, "Directional coupler formed by photonic crystal InAlGaAs nanorods," *J. Lightw. Technol.*, vol. 26, no. 5, pp. 488–491, Mar. 2008.

[32] C. C. Chen, C. Y. U. Chen, W. K. Wang, F.-H. Huang, C. K. Lin, W. Y. Chiu, and Y. J. Chan, "Photonic crystal directional couplers formed by InAlGaAs nano-rods," *Opt. Exp.*, vol. 13, no. 1, pp. 38–43, Jan. 2005.

[33] L. Ferrier, O. El Daif, X. Letartre, P. R. Romeo, C. Seassal, R. Mazurczyk, and P. Viktorovitch, "Surface emitting microlaser based on 2D photonic crystal rod lattices," *Opt. Exp.*, vol. 17, no. 12, pp. 9780–9788, Jun. 2009.

[34] Z. Qiang, W. Zhou, R. A. Soref, and Z. Ma, "Ultra-compact polymer and silicon modulator design based on photonic crystal ring resonators," in *Proc. SPIE*, 2008, vol. 6896, p. 68 960B.

[35] W.-Y. Chiu, T.-W. Huang, Y.-H. Wu, Y.-J. Chan, C.-H. Hou, H.-T. Chien, and C.-C. Chen, "A photonic crystal ring resonator formed by SOI nano-rods," *Opt. Exp.*, vol. 15, no. 23, pp. 15 500–15 506, Nov. 2007.

[36] RSoft Inc, RSoft Photonics CAD Suite. [Online]. Available: http://www.rsoftdesign.com

[37] S. S. Lo, M. S. Wang, and C. C. Chen, "Semiconductor hollow optical waveguides formed by omnidirectional reflectors," *Opt. Exp.*, vol. 12, no. 26, pp. 6589–6593, Dec. 2004.

[38] S. G. Johnson, C. Manolatou, S. H. Fan, P. R. Villeneuve, J. D. Joannopoulos, and H. A. Haus, "Elimination of cross talk in waveguide intersections," *Opt. Lett.*, vol. 23, no. 23, pp. 1855–1857, Dec. 1998.

[39] Y. Jiao, S. F. Mingaleev, M. Schillinger, D. A. B. Miller, S. Fan, and K. Busch, "Wannier basis design and optimization of a photonic crystal waveguide crossing," *IEEE Photon. Technol. Lett.*, vol. 17, no. 9, pp. 1875–1877, Sep. 2005.

[40] D. Wei-Qiang, T. Dong-Hua, C. Li-Xue, Z. Yuan, and L. Yan, "Photonic crystal waveguide intersection based on self-imaging of multi-mode interference," *Chin. Phys. Lett.*, vol. 24, no. 1, pp. 127–130, Jan. 2007.

[41] J. Chan, A. Biberman, B. G. Lee, and K. Bergman, "Insertion loss analysis in a photonic interconnection network for on-chip and off-chip communications," in *Proc. 21st Annu. Meet. IEEE LEOS*, Nov. 9–13, 2008, pp. 300–301.

[42] T. Fukazawa, T. Hirano, F. Ohno, and T. Baba, "Low loss intersection of Si photonic wire waveguides," *Jpn. J. Appl. Phys.*, vol. 43, no. 2A, pp. 646–647, Feb. 2004.

[43] R. Ji, L. Yang, L. Zhang, Y. Tian, J. Ding, H. Chen, Y. Lu, P. Zhou, and W. Zhu, "Microring-resonator-based four-port optical router for photonic networks-on-chip," *Opt. Exp.*, vol. 19, no. 20, pp. 18 945–18 955, Sep. 2011.

[44] X. Tan, L. M.Yang, L. Zhang, and J. Jiang, "On a scalable, non-blocking optical router for photonic networks-on-chip designs," in *Proc. SOPO*, May 2011, pp. 1–4.

[45] L. Ramini and D. Bertozzi, "Power efficiency of wavelength-routed optical NoC topologies for global connectivity of 3D multi-core processors," in *Proc. NoCArc*, 2012, pp. 25–30.

[46] L. Ramini, P. Grani, S. Bartolini, and D. Bertozzi, "Contrasting wavelength-routed optical NoC topologies for power-efficient 3D-stacked multicore processors using physical-layer analysis," in *Proc. DATE*, Grenoble, France , Mar. 18–22, 2013, pp. 1589–1594.

[47] N. Kirman and J. F. Martinez, "A power-efficient all-optical on-chip interconnect using wavelength-based oblivious routing," *ACM SIGARCH Comp. Architect. News*, vol. 38, no. 1, pp. 15–28, Mar. 2010.